

Predicting Eye Gaze Location on Websites

Ciheng Zhang¹, Decky Aspandi², Steffen Staab^{2,3}

¹*Institute of Industrial Automation and Software Engineering, University of Stuttgart, Stuttgart, Germany*

²*Institute for Parallel and Distributed Systems, University of Stuttgart, Stuttgart, Germany*

³*Web and Internet Science, University of Southampton, Southampton, United Kingdom*
st169011@stud.uni-stuttgart.de, {decky.aspandi-latif, steffen.staab}@ipvs.uni-stuttgart.de

Keywords: Eye-Gaze Saliency, Image Translation, Visual Attention

Abstract: World-wide-web, with the website and webpage as the main interface, facilitates the dissemination of important information. Hence it is crucial to optimize them for better user interaction, which is primarily done by analyzing users' behavior, especially users' eye-gaze locations. However, gathering these data is still considered to be labor and time intensive. In this work, we enable the development of automatic eye-gaze estimations given a website screenshots as the input. This is done by the curation of a unified dataset that consists of website screenshots, eye-gaze heatmap and website's layout information in the form of image and text masks. Our pre-processed dataset allows us to propose an effective deep learning-based model that leverages both image and text spatial location, which is combined through attention mechanism for effective eye-gaze prediction. In our experiment, we show the benefit of careful fine-tuning using our unified dataset to improve the accuracy of eye-gaze predictions. We further observe the capability of our model to focus on the targeted areas (images and text) to achieve high accuracy. Finally, the comparison with other alternatives shows the state-of-the-art result of our model establishing the benchmark for the eye-gaze prediction task.

1 INTRODUCTION

The analysis of user behavior during their interaction with website (and consisted webpages) is important to evaluate their overall quality. This information can be used to create a more optimized webpages for better interactions, as such, there are need to characterize these behaviors. Some of the characteristics include the tendency to focus on certain areas (e.g. upper left corner (Shen and Zhao, 2014)) during browsing. Other important characteristics can be defined from the user eye-gaze data - which normally represents the visual attention of the users during website interaction. This data is usually acquired from the human pupil-retinal location and movement relative to the object of interest allowing us to pinpoint the exact webpage area, where the users focus during their interactions and its relations with the overall webpage structure. Although this information is crucial to create a more optimized website for better interactions. However, Acquiring these eye-gaze data on each user during their browsing duration is difficult, given the complexity of the setting for the acquisition. Thus there is currently a need for an automatic approach to predict these eye-gaze locations given the observation

of the webpages.

In the computer vision field, saliency prediction task has been extensively investigated that allows one to estimate people's attention given an image. The main task is to estimate the saliency map, which highlights the first location (or region) where the observers' eyes focus, with the photographs of natural scenes (Zhang et al., 2018) (Kroner et al., 2020) commonly used as the input. Number of approaches have been developed so far to solve this task, including machine learning (Hou and Zhang, 2008) (Li et al., 2012) and recently deep learning based approaches (Kroner et al., 2020) with quite a high accuracy achieved. With this progress, there is an opportunity to adopt these automatic, visual based saliency predictors for eye-gaze predictions task, by representing the input observation in the form of website screenshot. This allows for the adaptation of task objective to be eye-gaze heatmap prediction, in lieu of saliency map, with both predicted map representing the area where the most people (or in our case users) attend.

The challenge however are the differences between these two prediction tasks in terms of the content, structure and layout. For instance, there is not

any concept of depth on website-screenshot as opposed to natural images, the aspect that is highly utilized for general visual saliency estimation. In addition, the high contrast and varied colored areas on the natural image are commonly regarded as saliency area, which may not be the case for website screenshots, given that user eye-gaze locations are highly dependent on the type of interactions during website browsing. This can be addressed by the use of a data-driven approach (Pan and Yang, 2010), which can be made feasible through fine-tuning using a specialized dataset on a particular task. However, this attempt is currently hampered by the lack of such dataset.

In this work, we curate a generalized dataset of eye-gaze prediction from website screenshots to enable effective training for machine and deep learning approaches. Using this dataset, we propose an effective deep learning based method that incorporates image and textual locations of the website through mask modalities and combines them with effective attention fusion mechanism. We then evaluate the impact of transfer learning, including comparison with other alternatives to establish a benchmark for this task. Specifically, the contributions of this work are:

1. The establishment of unified benchmark datasets for eye-gaze detection from website screenshots, derived from user interactions data.
2. A novel deep learning-based and multi-modal eye-gaze detector with internal attention that leverages the characteristics of input contents and the importance of each stream of modality for effective predictions.
3. Benchmark results of the automatic eye-gaze location estimator and our state-of-the-art results for the eye-gaze detection task given website screenshot inputs.

2 RELATED WORK

An early example of the work analyzing the website content is done by Zhao et.al. (Shen and Zhao, 2014) where three types of webpages are analyzed: Text-based, Pictorial-based, and Mixed (combination of Text and Pictorial) websites. The author showed that some attention characteristics of the users during the interactions with the webpage exist, with the main finding that people usually pay more attention to some relevant part of the websites (such as the left-top corner of a website) and people tend to focus on areas where large images are present. Specifically, on the websites from the ‘Text’ category, a user’s preference to focus on certain parts of the websites (the

middle left and bottom left regions) is perceived. In addition, they propose multi-kernel machine learning inferences for eye-gaze heatmap predictions (which represents the user’s visual attention) for their developed website eye-gaze dataset of Fixations in Webpage Images dataset (FiWI).

In the computer vision field, the task of locating (or predicting) user attention to the input natural image is commonly called as saliency prediction. These tasks are originally solved by the use of machine learning techniques, given its automation capability. The earliest example of this method is Incremental Coding Length (ICL) (Hou and Zhang, 2008) that aims to predict the activation of saliency location by measuring the perspective entropy gain of each input feature (several image patches) as a linear combination of sparse coding basis function. Subsequently, Context-Aware Saliency Detection (CASD) is a saliency detection algorithm that leverages from the concept of dominant objects as additional context to improve their prediction (Goferman et al., 2011). Furthermore, D Houx et.al. (Houx et al., 2012) proposed an approach to the figure-ground separation problem using a binary and holistic image descriptor of Image Signature, which is defined as the sign function of the Discrete Cosine Transform (DCT) of an image. Subsequently, Hypercomplex Fourier Transform (HFT) (Li et al., 2012) is used to transform the input image to the frequency domain acquiring the saliency map. One recent work utilizes deep learning based methods, given their accurate estimations and ability to leverage the huge datasets (that are increasingly present). This model is based on the Encoder and Decoder structure with a pre-trained VGG network to predict the saliency maps (Kroner et al., 2020).

Even though all of the described methods work for general visual saliency predictions, however, their capability to predict users’ eye-gaze location on the webpage is not yet investigated, given the lack of dataset available. Thus in this work, we propose to create a unified dataset to allow for the development of automatic eye-gaze predictions of the website screenshot inputs, then use them to develop our deep learning based eye-gaze location predictor.

3 METHODOLOGY

3.1 Dataset Gathering and Processing

In this work, we search, process and curate a generalized eye-gaze dataset from the available datasets in the literature. Here, we focus on

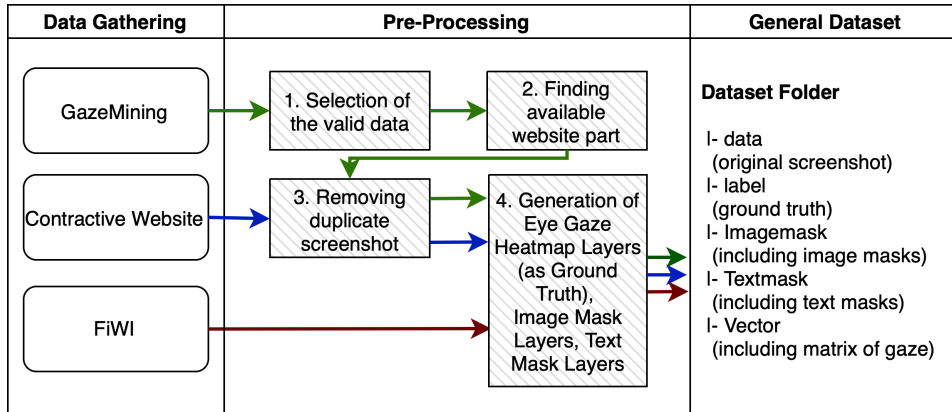


Figure 1: The flow of dataset generation.

the three publicly available user-website interaction datasets (where eye-gaze and webpage screenshots are present): GazeMining (Menges, 2020), Contrastive Website (Aspandi et al., 2022), and Fixations in Webpage Images (FiWI) dataset (Shen and Zhao, 2014). In this section, we provide a short description of the datasets, and proceed with the pre-processing algorithm that we conduct to produce the unified dataset. The processed dataset is available at ¹ and available after request.

- **GazeMining** is a dataset of video and interaction recordings on dynamic webpages (Menges, 2020). In this work, the authors focus on the websites which contain constantly changing scenes (thus dynamic). The data was collected on March 2019 from four participants who interacted with 12 different websites.
- **Contrastive Website dataset** is a recent website interaction-based dataset, where the participants were asked to visit two sets of websites (each of four) and performed respective tasks (flight planning, route search, new searching and on-line shopping) resulting on more than 160 sessions (Aspandi et al., 2022).
- **FiWI** dataset (Shen and Zhao, 2014) is the dataset that focuses on website-based saliency prediction. However, it is small in term of website screenshot availability (only 149 images) compared to two previous datasets that prevent its use for larger scale evaluations (this is especially true for a deep learning model). Therefore the FiWI dataset is mostly (and commonly) utilized as comparative evaluation with other models, but not for model training.

Figure 1 shows the flow of our dataset curation, data pre-processing and the results of the general-

¹<https://doi.org/10.18419/darus-3251>

ized dataset. The first step of the pre-processing is the elimination of the empty screenshots (which are frequently found on the GazeMining dataset), i.e. no screenshots present which can come due to rapid sampling during acquisition. Secondly, due to the dynamic nature of the observed websites, the webpage’s static parts are removed (or blackened) on the original datasets, which necessitates us to find and collect only the recorded screenshot - thus removing the irrelevant observations (black parts). Thirdly, we remove the duplicate webpage screenshots of both datasets for efficiency and generate the respective locations of Image and Text as independent layers (called Image and Text Mask, which we will detail in Section 3.2.1). Lastly, the eye-gaze heatmap layers are generated (as the ground truth) with respect to the duration of each observed eye-gaze. This pipeline is applied to all datasets, with the exception of Contrastive Website, where the first and second steps are skipped, and for the FiWI where only the last steps are necessary. In the end, our unified dataset includes five sub-folders (data, label, Imagemask, TextMask, Vector) with a total of 3119 screenshot examples and associated ground truth.

3.2 Multi Mask Input Attentional Network (MMIAN) for Eye Gaze Prediction

Our pre-processed data allow us to propose a deep learning based model to benefit from the sizable number of observations. Here we propose a Multi Mask Input Attentional Network (MMIAN) that aims to predict the eye gaze location given the website screenshot as input. Specifically, given input website screenshot images of $X_{i..n}$, with X as the 2D matrix of website screenshot image, and n as the number of batch size, MMIAN estimates the eye-gaze location of $\hat{Y}_{i..n}$,

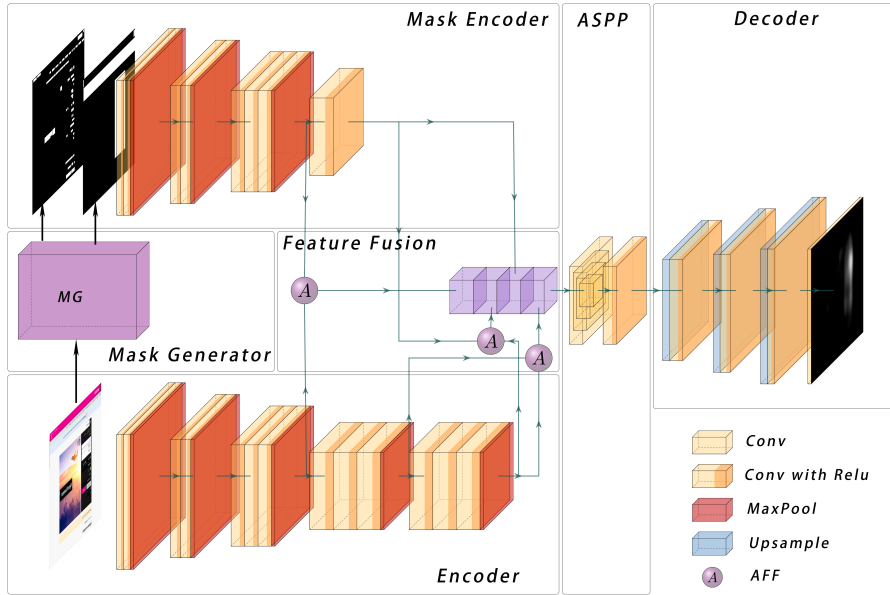


Figure 2: The structure of Multi Mask Input Attentional Network.

where each \hat{Y} is a 2D matrix of eye-gaze heatmap, with each cell value represents the probability of eye-gaze locations. The structure of MMIAN follows encoder-decoder scheme that is inspired by Multi-scale Information Network (MSI-Model) (Kroner et al., 2020) consisting of several modules: input and Mask Encoder, Mask Generator, Attentional Feature Fusion, Atrous Spatial Pyramid Pooling Module and Decoder. In this work, we further propose several important modifications:

1. The incorporation of several input masks to include webpage content information of textual and images spatial location.
2. The addition of attention mechanisms for effective fusion of input modalities.

The overall architecture can be seen in Figure 2. Specifically, an input website screenshot image is passed into the mask generator to produce an image mask and text mask. Then both masks are concatenated and passed into the Mask Encoder to extract relevant features, while the input image is simultaneously fed into the input Encoder. Feature Fusion module then fuses the extracted mask features and input features with several attentional modules and combines them in a conjoint block. This feature block is then fed into the ASPP part to enlarge the field of views to capture different resolution views from the input, producing a richer representation. This representation is then passed through the series of up-sampling layers (Decoder) creating an eye-gaze saliency map as a final result. The implementation

code of our model is available on our repository².

3.2.1 Input Masks Generator

It has been observed that the webpage layout (which in principle is the arrangement of images and texts) is an important aspect of the webpage (Shen and Zhao, 2014). To benefit from this information, we propose to incorporate spatial locations of both image and text on the websites with mask representations: image and text masks. These masks are represented in the form of a matrix, where each cell is activated in the presence of both image and text in the website screenshot.

- **Image Mask Generation:** For image location recognition, we used the method from M. Xie et al. (Xie et al., 2020), (Siedlecki and Sklansky, 1993), (Burtsev and Kuzmin, 1993) which produces bounding-box locations of existing image in a binary map (i.e. the map value is set to 1 where the image is present, otherwise 0).
- **Text Mask Generation:** we use one of the available optical character recognition (OCR) methods of Efficient and Accuracy Scene Text detection (EAST) (Zhou et al., 2017) to locate the location of the text of the website screenshot input. Similar to Image Mask, this process generates the corresponding Text Mask in Binary map format.

The example of the generated masks from our curated dataset can be seen in Figure 3. We can see that both of the masks contain quite accurate locations

²<https://github.tik.uni-stuttgart.de/ac138165/WebToGaze>

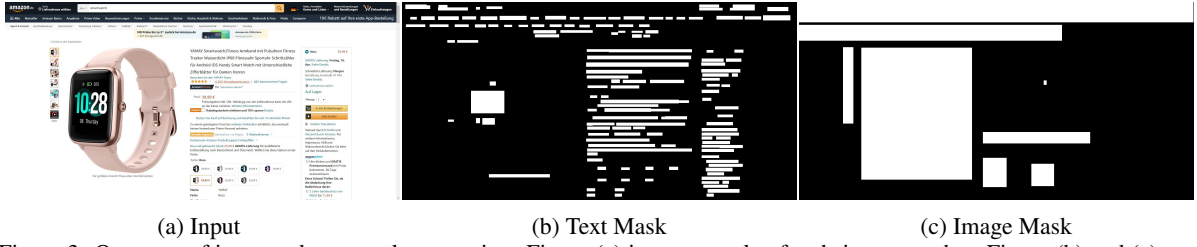


Figure 3: One case of input and text mask generation. Figure (a) is an example of website screenshot, Figure (b) and (c) are the generated text mask and image mask respectively.

of both Image and Text on the input website screenshots. Even though some mild imperfections occur (i.e. some buttons can be recognized as images, it does not fully detect the locations of certain images due to small size, and some text within the images are included on the text masks), however in general the locations of both image and text on the input website screenshots are properly recognized. These masks are then concatenated to be fed into Mask Encoder part.

3.2.2 Input and Mask Encoder

The Encoder part is the series of Convolutional Neural Network that aims to extract visual features from the input matrix, which is the original web screenshot image and concatenated generated Masks, for Input and Mask Encoder respectively. Both Encoders are based on the VGG16 (Simonyan and Zisserman, 2014) architectures with last fully connected layer removed, and further reductions of convolution layers (5 convolutional layers with Relu and two max-polling layers) applied for Mask Encoder. The Input and Mask encoder then produce the MaskFeatures and Screenshot Features to be combined through the Multi-Modal Attentional Fusion module.

3.2.3 Multi-modal Attentional Fusion

We introduce the attentional fusion mechanism for more effective modality fusion, as opposed to simple fusing operations, such as summation or concatenation and further solve the problems of inconsistent input semantics and scales (Dai et al., 2021). An example of the attentional feature fusion block (AFF) can be seen in Figure 4 where it receives two streams of inputs (denoted as $F1$ and $F2$) and initially fuses the feature through matrix addition (denoted as \oplus). The result from addition of the internal Multi-scale Channel Attention module (that aggregates the channel context by a series of point-wise convolutions) and a sigmoid function generates a fusion weight. This fusion weight and its other counterpart (where it is negated by one) are multiplied (denoted as \otimes) by each of original inputs respectively, and then added

together (\oplus symbol) to produce a weighted average to produce the fused feature Z . This fusion process is applied to the received MaskFeatures and Screenshot Features three times, to allow for the observation of different scales of the respective features (these operations are marked as circled A in the Figure 2). The resultants of the fused features are then concatenated to a conjoint block for the subsequent pipelines.

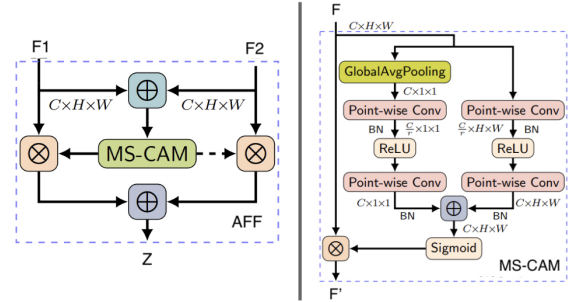


Figure 4: Left is Attentional Feature Fusion block, right is Multi-scale Channel Attention module (Dai et al., 2021).

3.2.4 Atrous Spatial Pyramid Pooling Module (ASPP)

ASPP module is made by superimposing different atrous convolutions (Chen et al., 2017) to obtain features from larger receptive fields. This is beneficial given that is common for webpage layouts to be modularized into a variety of different sub-layouts. Thus increasing the receptive fields (or field-of-view) of the internal convolutional filter allows us to capture such layout configurations. We implement this in our ASPP module with dilation rates of 4, 8, and 12, with the number of 1×1 filter to be 256 to ensure kernel size compatibility. This module is applied to the conjoint block, and subsequent features are obtained for the decoding operation.

3.2.5 Output Decoder

The Decoder part consists of a series of convolution layers with up-sampling to decode the input features,

generating the final prediction of eye-gaze heatmap location (in the form of a 2D tensor and in binary mode). Specifically, number of up-sampling blocks consisting of bilinear scaling operations (each sequentially doubles the number of input tensor) and a subsequent convolutional layer with kernel size 3×3 are used. With this module, we give the features generated from ASPP as the input features, and final eye-gaze heatmap predictions are obtained. Finally, we convert the binary heatmap to gray-scale format, to conform to original scale of eye-gaze heatmap ground-truth map.

3.3 Models' Training

To evaluate the impact of the training of the models utilizing website screenshot based eye-gaze prediction datasets, first we perform training process using an original saliency prediction model of Kroner's Model (MSI-Model) (Kroner et al., 2020). This model has been pre-trained on general visual saliency dataset (SALICON) (Jiang et al., 2015), which we call as P-MSI, that serves as the baseline. Given this pre-trained model, we do a fine-tuning using our pre-processed datasets (GazeMining and Contrastive Website dataset) producing FT-MSI-GM and FT-MSI-CW respectively, and evaluate the observed accuracy gains. Additionally, we propose to evaluate the impact of the training using the combined dataset (i.e. we combine the examples of both of GazeMining and Contrastive Website) by further training the MSI-Model with this merged dataset, that we will name as FT-MSI-CMB. The training is conducted until convergence and no further accuracy improvement is perceived.

Afterward, we proceed to the training stage of our proposed model of MMIAN by first transferring the Encoder and Decoder's weight from the best performing models of the previous step, and initialized weights of both Mask Encoder and ASPP by the zero-mean uniform distribution.

All of the training is conducted by minimizing Kullback-Leibler divergence (KLD) loss function as shown in Equation 1, with Y indicating the ground truth and ϵ is a regularization constant to guarantee that the denominator is not zero. In this loss, the estimation of saliency maps can be regarded as a probability distribution prediction task, as formulated by Jetley et. al. (Jetley et al., 2016). The output of the estimator is normalized to a non-negative number, with KLD value used to measure level of differences between predictions and ground truth. Finally, Adam optimizer (Kingma and Ba, 2014) with a learning rate of 10^{-4} is used for overall optimization.

$$D_{KL}(\hat{Y}||Y) = \sum_i Y_i \ln(\epsilon + \frac{Y_i}{\epsilon + \hat{Y}_i}) \quad (1)$$

3.4 Experiment Setting

3.4.1 Dataset Experiment Setting

In this experiment, all of the three pre-processed datasets (cf. Section 3.1) are utilized, with the training, validation and test instance numbers shown in Table 1. Specifically, both GazeMining and Contrastive Website datasets are divided with 60%, 20% and 20% of samples for the training, validation set, and test set respectively. Whereas for FiWI dataset (Shen and Zhao, 2014), all samples (of 149 images) are used for testing.

| Splits | GazeMining | Contrastive Website | FiWI |
|------------|------------|---------------------|------|
| Training | 928 | 868 | - |
| Validation | 309 | 278 | - |
| Test | 309 | 278 | 149 |

Table 1: Training, validation and test set for each dataset.

3.4.2 Quantitative Metrics

We use three quantitative metrics of Area under Receiver Operating Characteristic curve (AUC), Normalized Scanpath Saliency (NSS), and Person's Correlation Coefficient (CC) to judge the quality of the models' prediction.

- **NSS** is commonly used for general saliency prediction tasks as a direct correspondence measure between the predicted saliency maps and ground truth, which is computed as the average normalized saliency at fixated locations (Peters et al., 2005). Furthermore, NSS is sensitive to false positives, relative differences in saliency across the evaluated image, and general monotonic transformations (Bylinskii et al., 2018). With Y^B as a binary map of true fixation location and N to indicate the total pixel number and i indicates each pixel instance, the NSS value can be calculated using the equation below:

$$NSS(\hat{Y}, Y^B) = \frac{1}{N} \sum_i \hat{Y}_i \times Y_i^B \quad (2)$$

- **AUC-J** evaluates the predicted eye-gaze heatmaps as a classification task, where each prediction pixel is evaluated through a binary classification setting. Here, a certain threshold value used to decide whether it is deemed to be correctly predicted as eye-gaze locations, thus emphasizing the frequency of true positive. We use method described

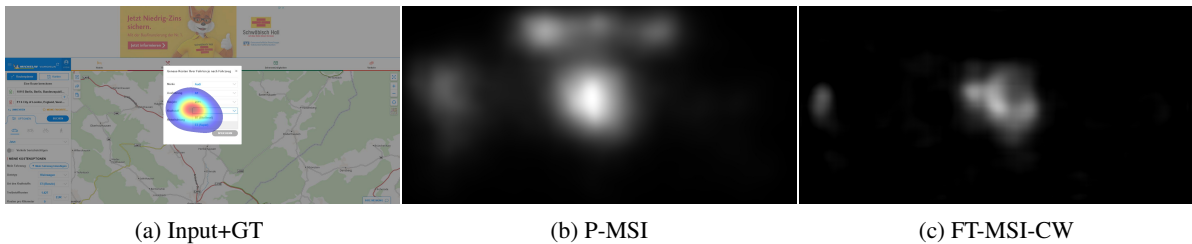


Figure 5: Comparison between pre-trained results from P-MSI (baseline) and FT-MSI-CW (Fine-tuned). Figure (a) shows the input screenshot with eye-gaze heatmap ground truth. Figure (b) and (c) shows predictions from P-MSI and FT-MSI-CW.

| No. | Models | GazeMining | | | Contrastive Website | | |
|-----|------------|--------------|--------------|--------------|---------------------|--------------|--------------|
| | | NSS | AUC-J | CC | NSS | AUC-J | CC |
| 1. | P-MSI | 1.037 | 0.699 | 0.130 | 0.839 | 0.683 | 0.109 |
| 2. | FT-MSI-GM | 1.398 | 0.753 | 0.170 | 0.717 | 0.651 | 0.093 |
| 3. | FT-MSI-CW | 0.695 | 0.655 | 0.081 | 2.364 | 0.777 | 0.277 |
| 4. | FT-MSI-CMB | 1.447 | 0.752 | 0.170 | 2.269 | 0.789 | 0.269 |

Table 2: The results of the fine-tuning model on both pre-processed GazeMining and Contrastive Website datasets.

by Judd et. al. (Judd et al., 2009) to select all required thresholds.

- **CC** metric aims to evaluate the linear relationship between two input distributions. In the eye-gaze location prediction task, both generated eye-gaze location map and the ground truth are treated as random variables (Le Meur et al., 2007), and the level of the linear relationship is calculated with both of these map inputs following equation 3. Thus, with operator σ as the covariance matrix, the CC value can be calculated as:

$$CC(\hat{Y}, Y) = \frac{\sigma(\hat{Y}, Y)}{\sigma(Y) \times \sigma(\hat{Y})} \quad (3)$$

4 EXPERIMENT RESULT

In this section, we first present the results of both baseline and our proposed approach using part of our pre-processed dataset (GazeMining and Contrastive Website), as outlined in Section 3. Then, we provide the comparison of the best results of our approaches with alternative saliency prediction models using the full set of our pre-processed dataset, establishing the benchmarking for the eye-gaze prediction task given website screenshot inputs.

4.1 The impact of Fine-tuning using independent and combined dataset.

Table 2 shows the results of four alternative models that are trained using different datasets. Here we can see that the pre-trained MSI (P-MSI) model performs worse in comparison to other models, which suggests

its inability to generalize to the eye-gaze saliency prediction task. We can further observe that when fine-tuning is applied, the improvement from the original P-MSI is noticeable, especially when it is tested on the similar dataset. This can be seen with the higher values of all metrics of FT-MSI-GM and FT-MSI-CW compared to P-MSI on the GazeMining dataset and Contrastive Website dataset respectively.

When the model is trained using combined dataset, however, the quality of predictions is instead reduced. This is indicated by the lower quantitative values achieved by the FT-MSI-CMB as opposed to their counterparts (FT-MSI-GM and FT-MSI-CW), that is trained separately. This phenomenon may come from the difficulty of the model to learn from these two datasets, which are quite distinct and can come from the nature of the task executed of each dataset.

Figure 5 presents visual prediction examples for the baseline model (P-MSI) and best performing model (FT-MSI-CW) for the Contrastive Website Dataset (where the example is originated). The screenshot example is a part of the route search task, where the user has to enter vehicle information to estimate fuel consumption. Thus it is natural for users to focus on the dialog box (displayed in the center of the website screenshot) resulting in the users' fixations being located within this area.

By evaluating the predictions of eye-gaze heatmaps of the baseline model of P-MSI, we can see that even though it manages to predict part of the ground-truth locations, however, it also falsely predicts other locations as eye-gaze locations (i.e. the advertisement part). These results can come from its tendency to detect the high color contrast as the area of interest, which is common in natural image datasets (SALICON (Jiang et al., 2015)). However, this leads to higher occurrences of false positive, thus reducing its accuracy. Our fine-tuned model however, manages to reduce the existing inaccuracies by absorbing the characteristics of the dataset during fine-tuning, adapting the model to this specific eye-gaze prediction task. In this example, we see that

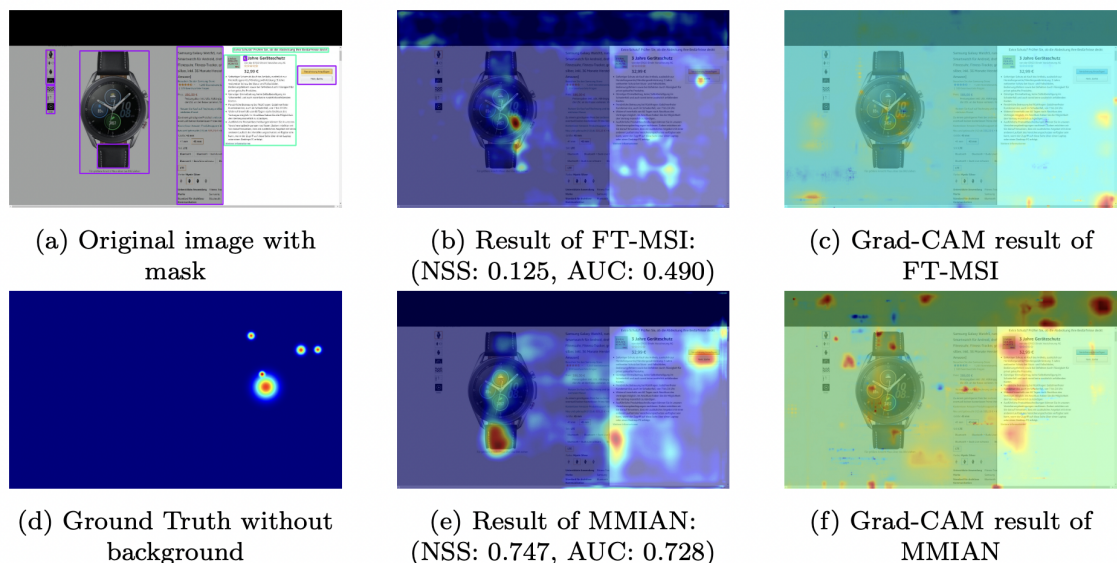


Figure 6: Example of the prediction results of MMIAN and Fine-tuned MSI Model (FT-MSI). The first column of (a) and (d) shows the website screenshot with outlined text (light green box) and image (purple box) area, along with the eye-gaze heatmap ground truth. The second column (b) and (e) shows the predicted result from FT-MSI and MMIAN model, with the third column of (c) and (f) shows respective Grad-CAM heatmap.

the model’s prediction is more precise, especially on the dialog box and exclude some of high contrast area that are normally recognized as saliency area (including advertisement locations).

From the experimental result, it can be concluded that the saliency detection model trained on the natural image dataset does not work well for direct application to the web screenshot scenario. This can be mitigated by performing careful fine-tuning to only use a dedicated dataset. Given this result, then we use the FT-MSI-GM and FT-MSI-CW as the base for MMIAN optimization, and for comparison in the next section.

4.2 Impact of Multi-modal Masks and Attention-based Fusion

| No. | Models | GazeMining | | | Contrastive Website | | |
|-----|--------|--------------|--------------|--------------|---------------------|--------------|--------------|
| | | NSS | AUC-J | CC | NSS | AUC-J | CC |
| 1. | FT-MSI | 1.398 | 0.753 | 0.170 | 2.364 | 0.777 | 0.277 |
| 2. | MMIAN | 1.579 | 0.764 | 0.184 | 2.487 | 0.787 | 0.292 |

Table 3: The result of both fine-tuned MSI models and MMIAN model.

Table 3 presents the results of our proposed MMIAN model and the best results of the fine-tuned MSI-Model from the previous section. From this result, it can be seen that MMIAN produces higher value across quantitative metrics in overall, outperforming the results from fine-tuned MSI-Model. The

gains on all of these metrics altogether, suggest that the estimation results of MMIAN are more accurate compared to the best of FT-MSI results (from FT-MSI-GM and FT-MSI-CW), with improvements on both true positive (as judged by AUC-Judd) and false positive Instances (as evaluated by NSS and CC score).

In order to provide a more comprehensive analysis of the impact of the use of image and text Masks and attention mechanisms, we first show the locations of detected images and texts on website screenshot input to provide semantic explanations of their relevances for our MMIAN model to produce accurate predictions. Then, we implemented a Gradient-weighted Class Activation Mapping (Grad-CAM) (Selvaraju et al., 2017) by propagating the multiplied error and gradient to each convolutional layer, enabling us to investigate the relevant activation of convolutional kernels - with respect to image input - indicating the most prominent part of website screenshot for prediction. The example of the original website screenshot input that includes the image and text locations (drawn as bounding box), the associated eye-gaze location ground-truth, generated Grad-CAM and each prediction of fine-tuned MSI and MMIAN is shown in the Figure 6.

From the figure, first we can see that the prediction of the MMIAN is more accurate than FT-MSI, with larger and correctly identified eye-gaze area are present. This is especially noticeable in the area

| No. | Models | GazeMining | | | Contrastive Website | | | FiWi | | |
|-----|--------------------------------------|--------------|--------------|--------------|---------------------|--------------|--------------|--------------|--------------|--------------|
| | | NSS | AUC | CC | NSS | AUC | CC | NSS | AUC | CC |
| 1. | CASD (Goferman et al., 2011) | 0.567 | 0.653 | 0.064 | 0.419 | 0.614 | 0.053 | 0.680 | 0.732 | 0.233 |
| 2. | DCTS (Houx et al., 2012) | 0.479 | 0.618 | 0.053 | 0.256 | 0.552 | 0.035 | 0.541 | 0.671 | 0.195 |
| 3. | HFT (Li et al., 2012) | 0.707 | 0.644 | 0.088 | 0.534 | 0.593 | 0.067 | 0.740 | 0.737 | 0.251 |
| 4. | ICL (Hou and Zhang, 2008) | 0.485 | 0.518 | 0.057 | 0.192 | 0.490 | 0.030 | 0.444 | 0.618 | 0.162 |
| 5. | RARE (Riche et al., 2012) | 0.632 | 0.653 | 0.072 | 0.382 | 0.589 | 0.052 | 0.850 | 0.758 | 0.280 |
| 6. | SeoMilanfar (Seo and Milanfar, 2009) | 0.393 | 0.584 | 0.038 | 0.350 | 0.571 | 0.044 | 0.445 | 0.651 | 0.163 |
| 7. | SR (Hou and Zhang, 2007) | 0.566 | 0.639 | 0.062 | 0.510 | 0.612 | 0.062 | 0.635 | 0.714 | 0.216 |
| 8. | MKL (Shen and Zhao, 2014) | - | - | - | - | - | - | 1.200 | 0.702 | 0.382 |
| 9. | MMIAN (proposed) | 1.579 | 0.764 | 0.184 | 2.487 | 0.787 | 0.292 | 1.385 | 0.786 | 0.397 |

Table 4: Comparison of existing saliency predictors evaluated on the test sets of our full pre-processed dataset. The boldface indicated the best results, the red color implies the second-best results, and the third-best results are marked by blue.

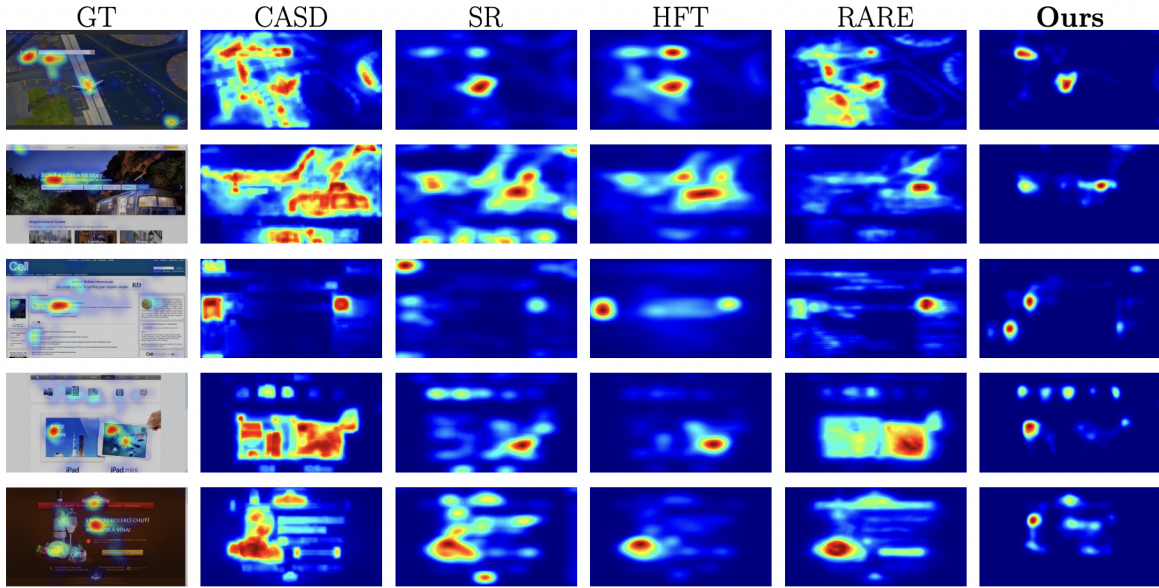


Figure 7: Five examples of screenshot inputs from FiWi dataset (with respective eye-gaze heatmaps ground-truth overlaid) and predictions from other five saliency predictors (including ours).

where both image and text are present. This can be seen in the areas where the button resides (that is recognized as image) and product description, which in this case, are indeed the locations where the user looks at). This perceived higher accuracy can be attributed to the use of the image and text masks during learning, which is combined effectively through attention mechanism to properly 'guide' the learning to put priority in this area. This impact is also apparent from the observation of the grad-cam heatmap of FT-MSI and MMIAN, where the grad-cam heatmap of MMIAN are seen to be more concentrated on both of the images and text area simultaneously (indicating where the models' attention is) as opposed to the ones produced by FT-MSI. Lastly, we also notice that there are more frequent activations of grad-cam heatmaps of MMIAN compared to FT-MSI, which may suggest that the larger perceptual field of view from MMIAN

is indicative to be able to produce more accurate eye-gaze estimations in overall.

4.3 State-of-the-Arts Comparison

We compare the best predictions of our approach against other seven generalized visual saliency models of Context-Aware Saliency Detection (CASD) (Goferman et al., 2011), Discrete Cosine Transform (DCTS) (Houx et al., 2012), Hypercomplex Fourier Transform (HFT) (Li et al., 2012), Incremental Coding Length (ICL) (Hou and Zhang, 2008), RARE (Riche et al., 2012), SeoMilanfar (Seo and Milanfar, 2009), Spectral Residual (SR) (Hou and Zhang, 2007), including one specialized eye-gaze location estimator of Multiple Kernel Learning (MKL) (Shen and Zhao, 2014).

Table 4 shows the results from all evaluated ap-

proaches. Here we see the state-of-the-art results of our MMIAN model that outperforms other alternatives, including eye-gaze predictor of MKL with a large margin on the FiWI dataset (note that there is no training involved for FiWI dataset evaluation). This result is mainly due to large differences in task characteristics between general visual saliency prediction (where the first seven models are trained) and website screenshot based eye-gaze estimations tasks (where MKL and MMIAN are specialized). This highlights the inability of visual saliency based models to generalize on this specific task. Furthermore, our model performs better than MKL on the FiWI, demonstrating the effectiveness of our overall approach for the eye-gaze estimation task.

Figure 7 shows the example of the predictions of our approach (MMIAN) and four other best performing model on FiWI for evaluation (excluding MKL, due to lack of the available implementation of the model). Based on this figure, we can observe that most alternative models produce a large area of the website screenshot as potential eye-gaze locations. However, this leads to in overall larger false positive, given the mismatch between the predictions against the actual eye-gaze locations from the user of these website screenshots (i.e. most area are falsely identified as eye-gaze locations). In contrast, our model produces more precise estimates, as observed by more refined (and accurate) predicted area of the eye-gaze locations (that explains the large margin in terms of NSS metrics from our models compared to others, as shown in Table 4). This is mainly due to the tendency of the general visual saliency model to focus on the pure appearance of the website screenshot (i.e. high contrast images), as opposed to MMIAN that has been conditioned to the specific characteristics of our pre-processed eye-gaze dataset (which inherently contains eye-gaze characteristics of the user, given website screenshot). Remarkably, our models is also capable of correctly predicting the eye-gaze locations on the relevant area, such as text (third row) and image (fourth column) and their combinations (first, second and fifth), in comparison to other models. Here we see that our models' predictions are consistently more accurate than the alternatives, demonstrating the effectiveness of our approach.

5 CONCLUSION

In this work, we enable the development of automatic eye-gaze estimations given website screenshot inputs to allow for the improvement of the webpage layout, and respective user interaction. We do this by devel-

oping a unified eye-gaze dataset from three available website and user interaction-based datasets: GazeMining, Contrastive Website and FiWI. We then pre-process each dataset to produce the necessary data for the eye-gaze prediction task, such as webpage screenshot and corresponding eye-gaze heatmaps as ground truth. In addition, we provide image and textual locations from the webpage (in the form of masks) which can be used for training and modeling. Given our unified eye-gaze dataset, then we proposed a novel deep learning based and multi-modal attentional network eye-gaze predictor to benefit from the characteristics of the dataset. Our proposed approach leverages the spatial locations of text and image (in form of masks), which is further fused with attentional mechanisms to enhance the prediction results.

During the analysis of the impact of fine-tuning using our pre-processed dataset, and the effects of the training when the combined dataset is used, we found that the prediction results are indeed improved when careful fine-tuning is conducted. Then, we evaluate the prediction of our full approach (MMIAN) with respect to the ground truth, existing text and image locations from the website screenshot, and part of the Grad-CAM activations. Here we notice accurate predictions of our approach, especially on the textual and image area where the user is looking, with large and wide activation of Grad-CAM that are also concentrated on these locations. This observation demonstrates the benefit of the use of both image and text masks as input in combination with the attention mechanism.

To measure the competitive results of our proposed approach, we compare the results of our model with other saliency prediction alternatives, establishing a benchmark for eye-gaze prediction task. In our comparison, we show state-of-the-art results of our model with a high score across quantitative metrics and a lower false positive rate than other approaches. Visual analysis further confirms our findings, that our approach produces more accurate prediction of eye-gaze locations on the relevant website locations, including where the text and image are present. The result suggests the benefit of our approach in capturing user behavior. The future work will be to incorporate other user behavior characteristics as additional modalities (e.g. mouse trajectory) to further benefit from this information to improve prediction accuracy.

ACKNOWLEDGEMENT

This work is funded by UDeco project by Germany BMBF-KMU Innovativ.

REFERENCES

- Aspandi, D., Doosdal, S., Ülger, V., Gillich, L., Menges, R., Hedeshy, R., Kumar, C., Schaefer, C., Walber, T., and Staab, S. (2022). User interaction analysis through contrasting websites experience. *arXiv preprint arXiv:2201.03638*.
- Burtsev, S. and Kuzmin, Y. P. (1993). An efficient flood-filling algorithm. *Computers & graphics*, 17(5):549–561.
- Bylinskii, Z., Judd, T., Oliva, A., Torralba, A., and Durand, F. (2018). What do different evaluation metrics tell us about saliency models? *IEEE transactions on pattern analysis and machine intelligence*, 41(3):740–757.
- Chen, L.-C., Papandreou, G., Kokkinos, I., Murphy, K., and Yuille, A. L. (2017). Deeplab: Semantic image segmentation with deep convolutional nets, atrous convolution, and fully connected crfs. *IEEE transactions on pattern analysis and machine intelligence*, 40(4):834–848.
- Dai, Y., Gieseke, F., Oehmcke, S., Wu, Y., and Barnard, K. (2021). Attentional feature fusion. In *Proceedings of the IEEE/CVF Winter Conference on Applications of Computer Vision*, pages 3560–3569.
- Goferman, S., Zelnik-Manor, L., and Tal, A. (2011). Context-aware saliency detection. *IEEE transactions on pattern analysis and machine intelligence*, 34(10):1915–1926.
- Hou, X. and Zhang, L. (2007). Saliency detection: A spectral residual approach. In *2007 IEEE Conference on computer vision and pattern recognition*, pages 1–8. Ieee.
- Hou, X. and Zhang, L. (2008). Dynamic visual attention: Searching for coding length increments. *Advances in neural information processing systems*, 21.
- Houx, D., HAREL, J., and KOCH, C. (2012). Image signature: highlighting sparse salient regions. *IEEE Transactions on Pattern Analysis and Machine Intelligence*, 34(1):194–201.
- Jetley, S., Murray, N., and Vig, E. (2016). End-to-end saliency mapping via probability distribution prediction. In *Proceedings of the IEEE conference on computer vision and pattern recognition*, pages 5753–5761.
- Jiang, M., Huang, S., Duan, J., and Zhao, Q. (2015). Sali-con: Saliency in context. In *Proceedings of the IEEE conference on computer vision and pattern recognition*, pages 1072–1080.
- Judd, T., Ehinger, K., Durand, F., and Torralba, A. (2009). Learning to predict where humans look. In *2009 IEEE 12th international conference on computer vision*, pages 2106–2113. IEEE.
- Kingma, D. P. and Ba, J. (2014). Adam: A method for stochastic optimization. *arXiv preprint arXiv:1412.6980*.
- Kroner, A., Senden, M., Driessens, K., and Goebel, R. (2020). Contextual encoder–decoder network for visual saliency prediction. *Neural Networks*, 129:261–270.
- Le Meur, O., Le Callet, P., and Barba, D. (2007). Predicting visual fixations on video based on low-level visual features. *Vision research*, 47(19):2483–2498.
- Li, J., Levine, M. D., An, X., Xu, X., and He, H. (2012). Visual saliency based on scale-space analysis in the frequency domain. *IEEE transactions on pattern analysis and machine intelligence*, 35(4):996–1010.
- Menges, R. (2020). Gazemining: A dataset of video and interaction recordings on dynamic web pages. labels of visual change, segmentation of videos into stimulus shots, and discovery of visual stimuli.
- Pan, S. J. and Yang, Q. (2010). A survey on transfer learning. *IEEE Transactions on Knowledge and Data Engineering*, 22(10):1345–1359.
- Peters, R. J., Iyer, A., Itti, L., and Koch, C. (2005). Components of bottom-up gaze allocation in natural images. *Vision Research*, 45(18):2397–2416.
- Riche, N., Mancas, M., Gosselin, B., and Dutoit, T. (2012). Rare: A new bottom-up saliency model. In *2012 19th IEEE International Conference on Image Processing*, pages 641–644. IEEE.
- Selvaraju, R. R., Cogswell, M., Das, A., Vedantam, R., Parikh, D., and Batra, D. (2017). Grad-cam: Visual explanations from deep networks via gradient-based localization. In *Proceedings of the IEEE international conference on computer vision*, pages 618–626.
- Seo, H. J. and Milanfar, P. (2009). Static and space-time visual saliency detection by self-resemblance. *Journal of vision*, 9(12):15–15.
- Shen, C. and Zhao, Q. (2014). Webpage saliency. In *European conference on computer vision*, pages 33–46. Springer.
- Siedlecki, W. and Sklansky, J. (1993). A note on genetic algorithms for large-scale feature selection. In *Handbook of pattern recognition and computer vision*, pages 88–107. World Scientific.
- Simonyan, K. and Zisserman, A. (2014). Very deep convolutional networks for large-scale image recognition. *arXiv preprint arXiv:1409.1556*.
- Xie, M., Feng, S., Xing, Z., Chen, J., and Chen, C. (2020). *UIED: A Hybrid Tool for GUI Element Detection*, page 1655–1659. Association for Computing Machinery, New York, NY, USA.
- Zhang, D., Fu, H., Han, J., Borji, A., and Li, X. (2018). A review of co-saliency detection algorithms: Fundamentals, applications, and challenges. *ACM Transactions on Intelligent Systems and Technology (TIST)*, 9(4):1–31.
- Zhou, X., Yao, C., Wen, H., Wang, Y., Zhou, S., He, W., and Liang, J. (2017). East: An efficient and accurate scene text detector. In *Proceedings of the IEEE Conference on Computer Vision and Pattern Recognition (CVPR)*.